



## Study of methyl orange adsorption properties on ZnO–Al<sub>2</sub>O<sub>3</sub> nanocomposite adsorbent particles

Hamid Tajizadegan\*, Omid Torabi, Azam Heidary, Mohammad Hosein Golabgir, Amin Jamshidi

*Young Researchers and Elite Club, Najafabad Branch, Islamic Azad University, P.O. Box 517, Isfahan, Iran, Tel./Fax: +98 31 4229 1008; emails: hamid\_tjz@yahoo.com (H. Tajizadegan), Omid\_trb@yahoo.com (O. Torabi), E.heidary\_2009@yahoo.com (A. Heidary), H22Golabgir@yahoo.com (M.H. Golabgir), Amin\_jam\_g@yahoo.com (A. Jamshidi)*

Received 14 December 2014; Accepted 4 May 2015

### ABSTRACT

The adsorption of methyl orange (MO) from an aqueous solution on the synthesized ZnO–Al<sub>2</sub>O<sub>3</sub> nanocomposite was investigated. The ZnO–Al<sub>2</sub>O<sub>3</sub> nanocomposite particles were composed of ZnO nanoflakes grown on the alumina particles (Al<sub>2</sub>O<sub>3</sub> core and ZnO shell). Under optimal conditions (MO concentration of 150 ppm, adsorbent concentration of 500 ppm, and the pH value of 4.5), the prepared nanocomposite showed adsorption capacity of 291 mg/g and the percentage removal of 97% at the equilibrium time of 30 min. It was found that the MO adsorption process was mainly controlled by intraparticle diffusion and film diffusion mechanisms which occurred simultaneously during the adsorption. The adsorption isotherm was well described by Langmuir isotherm model, which exhibited the maximum adsorption capacity of 344.83 mg/g. The obtained low-cost nanocomposite was proved to be a promising adsorbent for the removal of anionic dyes in industrial wastewater treatment.

*Keywords:* ZnO; Al<sub>2</sub>O<sub>3</sub>; Methyl orange; Kinetics; Adsorption isotherm; Dye removal

### 1. Introduction

Due to the loss of a large amount of dye materials during manufacturing and processing operations, the effluents of many dye consumer or producer industries such as tanning, textile, paper, leather, food processing, and dyestuff plants contain significant quantities of dye waste [1,2]. These dye wastes are hazardous, toxic, nonbiodegradable, and extremely carcinogenic. More importantly, these effluents are unfortunately discharged into the environment. Thus, survival of human beings mainly depends on removing dye pollutants from industrial effluents to minimize their

environmental impacts. Methyl orange (MO) is one of the common water-soluble azo dyes widely used in textile, paper, and chemical industries [1]. It is harmful to environment and human and, consequently, it is vital to treat it before it is discharged into the environment. Recently, due to prominent properties such as high efficiency, simplicity, and reusability, the adsorption method has been favored over other methods such as filtration, coagulation, chemical oxidation, sedimentation, ion exchange, and precipitation for dye removal from industrial wastewaters [3]. Traditionally, during past decades, activated alumina ( $\gamma$ -Al<sub>2</sub>O<sub>3</sub>) has been used as adsorbents in dye adsorption [4]. In addition, activated alumina has been extensively used as a support for adsorbents [5,6]. In contrast to traditional

\*Corresponding author.

adsorbents, nowadays there is a growing interest in using low-cost adsorbents, especially with higher yields. Thus, many researchers have been studying the use of alternative materials as adsorbents for dye removal process [7,8].

Zinc oxide (ZnO) has been generally used as photocatalyst in photocatalytic degradation of dye compounds in the presence of artificial UV light sources [9]. Nevertheless, ZnO has been used very meagerly as an adsorbent for dye removal with adsorption method. The morphology of ZnO has a great influence on its performance, especially in nanoscale [10]. Among various morphologies, ZnO nanosheets have attracted considerable attention due to polar surfaces with an activated surface charge, and also larger aggregation resistance (compared to spherical nanoparticles) [10,11]. Besides, due to the fact that adsorption reaction takes place on the surface of the solid phase of adsorbent, supporting nanosized ZnO on porous materials like activated alumina can be an effective way to increase the surface area and aggregation resistance of nanoZnO active species [12]. In other words, ZnO–Al<sub>2</sub>O<sub>3</sub> nanocomposite particles have certain advantages over commercially available adsorbents, mainly in terms of low-cost, high surface charge, and large contact area between dye molecules and active sites.

In a previous work, the authors synthesized ZnO–Al<sub>2</sub>O<sub>3</sub> nanocomposite particles via heterogeneous precipitation method with different ratios of ZnO to Al<sub>2</sub>O<sub>3</sub> [13]. To the best of our knowledge in previous work, it was believed that morphology in nanoscale is a measure of potential surface charges of the ZnO, and that surface area is a measure of how much of this potential can be released. It was concluded that the low-cost ZnO–Al<sub>2</sub>O<sub>3</sub> nanocomposite prepared with ZnO content of 40 wt% is the best efficient adsorbent for the removal of MO dye from aqueous solution. In the present work, efforts have been made to determine the optimum conditions for adsorption properties of MO (to serve as a model compound for common anionic water-soluble azo dyes) by the above-mentioned ZnO–Al<sub>2</sub>O<sub>3</sub> nanocomposite from aqueous solution. More specifically, the effects of various parameters on the removal of MO such as equilibrium time, MO concentration, adsorbent concentration, and the pH of solution are studied. Moreover, the adsorption isotherms and kinetic models are considered.

## 2. Experimental

### 2.1. Preparation and characterization of the adsorbent

ZnO–Al<sub>2</sub>O<sub>3</sub> adsorbent with ZnO content of 40 wt% was prepared via heterogeneous precipitation using

Al(OH)<sub>3</sub> particles as the seed. The detailed preparation procedure can be found in our previous work [13].

The morphology and microstructure of adsorbent were studied by field-emission scanning electron microscope (FE-SEM, Hitachi S-4160). The specific surface area ( $S_{BET}$ ) was measured by BET method using N<sub>2</sub> adsorption isotherms at 77 K (micromeritics ASAP-2010).

### 2.2. Batch adsorption experiments

MO (C<sub>14</sub>H<sub>14</sub>N<sub>3</sub>NaO<sub>3</sub>S) was supplied by Merck Co. and was used as received. The chemical structure of the dye is shown in Fig. 1. Batch adsorption experiments were carried out to examine the adsorption properties of the synthesized adsorbent for MO adsorption from an aqueous solution. Stock solutions of 1,000 mg/L (1,000 ppm) were prepared by dissolving MO powder in distilled water and in all steps of examination, the desired concentrations were obtained from diluting the stock solution. Adsorption experiments were carried out by varying the initial concentration of dye solution from 30 to 150 mg/L, the amount of adsorbent from 200 to 700 mg/L, and the pH from 2.6 to 10.1. The pH value was adjusted to a desired value by adding 0.1 mol/L of NaOH or HCl solution. In a typical experiment, the adsorbent with the preferred concentration was added to a glass flask containing 10 ml of the aqueous solution of MO. The mixture was magnetically stirred at room temperature and at a rate of 400 rpm. At predetermined time intervals, the mixture was centrifuged in order to separate the dye solution from the adsorbent, and then the residual concentration of MO was measured with a UV–vis spectrophotometer (Optizen 3220) at the wavelength of 465 nm. The amount of the MO adsorbed by ZnO–Al<sub>2</sub>O<sub>3</sub> composite adsorbent,  $q$  (in mg/g), as well as the percentage removal of MO ( $\eta$ ) were calculated by the following equations:

$$q = \frac{(C_0 - C_t)V}{m} \quad (1)$$

$$\eta = \frac{(C_0 - C_t)}{C_0} \times 100 \quad (2)$$

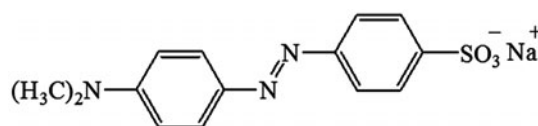


Fig. 1. The chemical structure of MO.

where  $C_0$  is the initial concentration of MO (in mg/L),  $C_t$  (in mg/L) is the instant concentration of MO at a predetermined time  $t$ ,  $V$  is the volume of the solution (in L), and  $m$  is the mass of adsorbent (in g). It should be mentioned that all experiments were carried out in triplicate.

### 3. Results and discussion

#### 3.1. Microstructural consideration of the adsorbent

With the aim of stabilizing the nanoZnO active species on the surfaces of  $\text{Al}_2\text{O}_3$  particles, heterogeneous precipitation method using seed particles was designed to synthesize  $\text{ZnO-Al}_2\text{O}_3$  nanocomposite particles. The greatest benefit of the synthesized  $\text{ZnO-Al}_2\text{O}_3$  nanocomposite was the promising increase in dye adsorption. Details of the synthesis method and affirmation of the adsorbent ability in MO dye adsorption have been previously reported [13]. However, in order to investigate the optimum conditions of adsorption and to give a more comprehensible account of the adsorption behavior, the authors present a brief study on the microstructure of the adsorbent. As can be seen in Fig. 2, the synthesized nanocomposite particles are composed of ZnO nanoflakes grown on the alumina particles ( $\text{Al}_2\text{O}_3$  cores, and ZnO shells with flake thickness of about 40–80 nm). The nitrogen adsorption–desorption isotherm of  $\text{ZnO-Al}_2\text{O}_3$  nanocomposite powder is depicted in Fig. 3 and its corresponding BJH pore size distribution is shown in the inset. As depicted, adsorption–desorption isotherm corresponds to the IUPAC type-IV pattern with an H3 hysteresis loop, indicating the existence of mesoporous structure in the adsorbent texture. Also, the BJH pore size distribu-

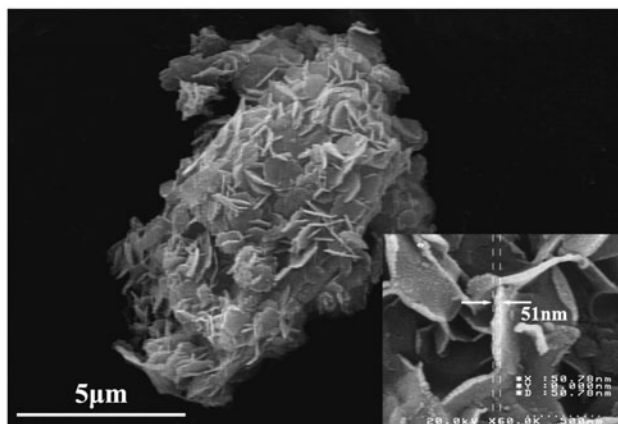


Fig. 2. FE-SEM micrograph of the synthesized  $\text{ZnO-Al}_2\text{O}_3$  nanocomposite particles.

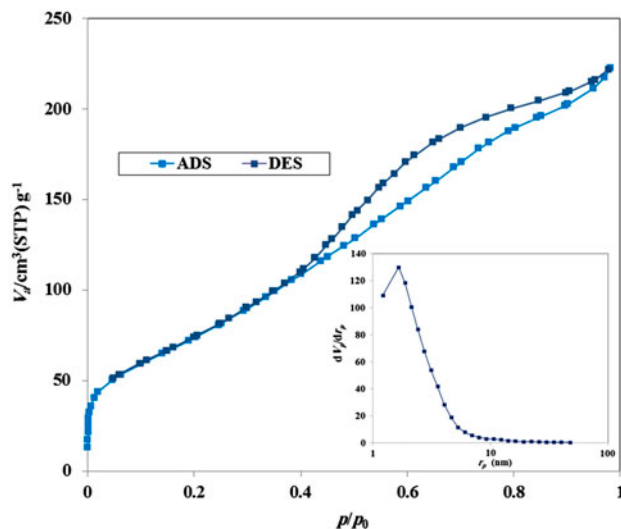


Fig. 3. Nitrogen adsorption–desorption isotherm of the  $\text{ZnO-Al}_2\text{O}_3$  nanocomposite particles. (The inset is the corresponding pore size distribution.)

tion plot shows ordered mesopores with diameters ranging between 2 and 10 nm. It should be mentioned that the mesoporous structure can play an important role in facile mass transfer of reactant molecules to the adsorbent surface. In addition, the surface area was measured to be about  $279 \text{ m}^2/\text{g}$ . The ZnO nanoflakes act as the nanosized active sites with a high surface charge. This means that anionic ions of MO can be adsorbed on the surfaces of ZnO active sites with positive charge [13]. It should be mentioned that this active surface charge of ZnO is caused by the formation of polar surfaces resulting from nonsymmetric structure of ZnO in plate shape morphology [10,11]. Furthermore, alumina particles with high surface area have a significant role in introducing these charged ZnO nanoflakes. In other words, alumina particles enhance the contact area between the active sites of ZnO and MO molecules in the adsorption process, which can be confirmed by measured BET surface area and microstructural observation.

#### 3.2. Effect of adsorbent concentration on adsorption

Fig. 4 shows the effect of adsorbent concentration (varied from 200 to 700 ppm) on dye removal efficiency of 50 ppm of MO solution. In all cases, the adsorption process quickly occurred at the initial contact time and became slower at further contact times. This rapid adsorption happens by the formation of a high gradient of MO concentration between the solution and solid phase at the initial contact times [14,15]. With the increase in contact time, the concentration

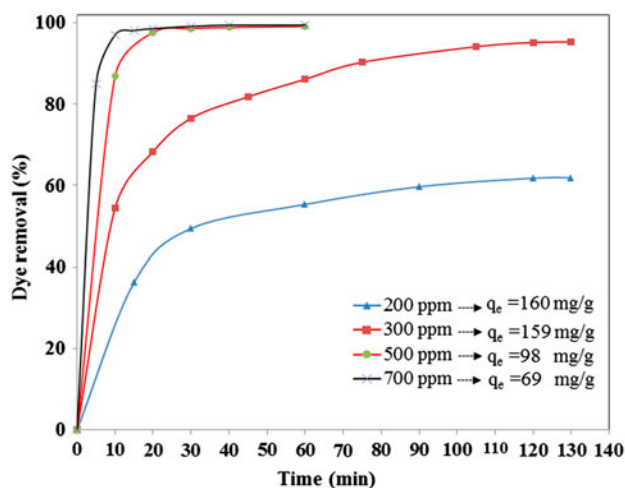


Fig. 4. Effect of adsorbent concentration on adsorption process (initial MO concentration of 50 ppm, pH of 6.5).

gradient of MO decreases by the progress of adsorption process, which leads to a slower ratio of adsorption. Also, by increasing the adsorbent concentration from 200 to 700 ppm, the dye removal efficiency increases from 62 to 98%, due to the more availability of adsorption sites and adsorbent surface area caused by more ZnO–Al<sub>2</sub>O<sub>3</sub> adsorbent particles. Furthermore, with an increase in adsorbent concentration from 200 to 700 ppm, the presence of more active sites facilitates the accessibility of MO molecules to adsorption sites. Thus, the adsorption reaches the equilibrium state at a shorter contact time (120–10 min, respectively), as shown in Fig. 4. The amount of adsorbed MO ( $q_e$  in mg/g) on unit weight of ZnO–Al<sub>2</sub>O<sub>3</sub> nanocomposite decreased from 160 to 69 mg/g as the adsorbent concentration increases from 200 to 700 ppm. This result is expected because of the splitting effect of concentration gradient between dye solution and solid phase caused by high proportion of active sites to dye molecules [14–16]. It should be mentioned that both cases of the adsorbent concentrations of 500 and 700 ppm can treat the dye solution with percentage removal of 98% in short times. Therefore, from an economic point of view, the adsorbent concentration of 500 ppm with 98% efficiency and adsorption capacity of 98 mg/g in equilibrium time of 20 min was chosen for the following experiments.

### 3.3. Effect of dye concentration on adsorption

To study the effect of initial dye concentration, the adsorption experiments were performed by changing the concentration from 30 to 150 ppm in dye solution, while the other parameters were kept constant. The

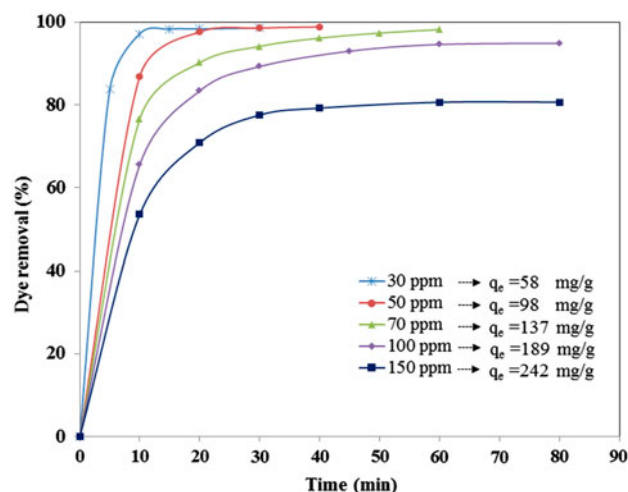


Fig. 5. Effect of dye concentration on adsorption process (adsorbent concentration of 500 ppm, pH of 6.5).

obtained results are presented in Fig. 5 in terms of percentage removal of MO from the aqueous solution as a function of time. The results revealed that the percentage removal of MO decreased with increasing the initial dye concentration after a certain concentration. It should be noted that, at a fixed concentration of ZnO–Al<sub>2</sub>O<sub>3</sub> particles, the amount of the available active sites and surface area in the adsorbent particles is constant, which would be saturated after a certain concentration [16,17]. As can be seen in Fig. 5, the cases of 30, 50, and 70 ppm can reach the percentage removal of 98% as they are below the saturated concentration, while the maximum percentage removal was 94% for 100 ppm and only 80% for 150 ppm, indicating that they are above the saturated concentration. Moreover, as the initial MO concentration increases from 30 to 150 ppm, the equilibrium time increases from 10 to 60 min and the adsorption capacity increases from 58 to 242 mg/g. Enhancement in the equilibrium time with increasing the initial MO concentration can be explained by the fact that more presence of MO molecules in the solution (at fixed adsorbent concentration) leads to more mass transfer resistance, which evidently requires more time for adsorption to overcome this mass transfer resistance of MO molecules at higher concentrations. Besides, by increasing the initial MO concentration, the concentration gradient of MO between dye solution and solid phase increases. As a result, it acts as a driving force for the transfer of MO molecules to the adsorbent surface [3,14]. The enhancement in adsorption capacity by increasing the MO concentration was attributed to higher driving force for mass transfer and utilization of all active sites for adsorption. From an economic

point of view, the dye concentration of 150 ppm with 80% efficiency and adsorption capacity of 242 mg/g in equilibrium time of 60 min was chosen for the following experiments.

### 3.4. Effect of the solution pH on adsorption

In order to clarify the effect of solution pH on the removal efficiency and adsorption capacity, a series of adsorption experiments with different pH values varying from 2.6 to 10.1 were performed under the same conditions. The obtained results are plotted in Fig. 6. It was found that both percentage removal and adsorption capacity quickly decrease by enhancing the pH value. More particularly, it was 56% efficiency with adsorption capacity of 169 mg/g for pH value of 8.2, and only 40% efficiency with adsorption capacity of 122 mg/g for pH value of 10.1. Also, it is further noted that the percentage of MO removal and the amount of adsorbed MO on ZnO–Al<sub>2</sub>O<sub>3</sub> nanocomposite particles are high for weak acid pH, i.e. in the range from pH value of 3 to 7. The adsorption capacity and the maximum percentage removal were achieved for the pH value of 4.5, while it was calculated about 97% efficiency and adsorption capacity of 291 mg/g in equilibrium time of 30 min. In order to determine the surface characteristic of the adsorbent, the zeta potential of ZnO–Al<sub>2</sub>O<sub>3</sub> nanocomposite was measured. Measurements indicated that this material has a net zero charge at pH value of 6.1 and positive surface at pH values below the zero point. Hence, as the pH value increases, zeta potential of the nanocom-

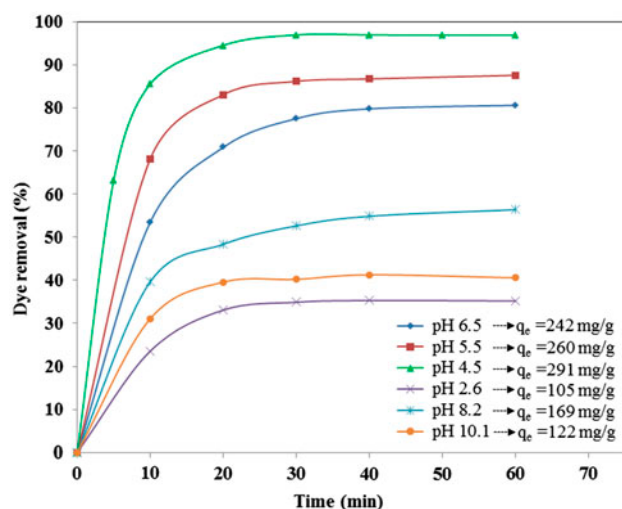


Fig. 6. Effect of solution pH on adsorption process (adsorbent concentration of 500 ppm, MO concentration of 100 ppm).

posite decreases and the surface of the nanocomposite is negatively charged. Meanwhile, it should be mentioned that MO dye is an anionic dye with a negative charge (Fig. 1). Thus, in higher basic pH, there is a severe competition between MO and hydroxyl ions for adsorption sites on ZnO nanoflakes with positive charge. As a result, the number of positively charged active sites on adsorbent is reduced, which relatively leads to negatively charged surfaces for ZnO–Al<sub>2</sub>O<sub>3</sub> nanocomposite particles. Consequently, the significant reduction in the MO removal and adsorption at higher basic pH was contributed to electrostatic repulsion between the negatively charged ZnO–Al<sub>2</sub>O<sub>3</sub> nanocomposite particles and MO anions, caused by the presence of excess hydroxyl ions. Furthermore, the greater adsorption at lower acid pH can be first corresponded by positively charged surface sites of ZnO nanoflakes and higher zeta potential in this range. Also, in acidic pH, the MO molecules are easily ionized to a soluble MO anion, which facilitates the diffusion of MO anion toward the adsorption sites of adsorbent surface [14,18,19]. Also, the surface charge of Al<sub>2</sub>O<sub>3</sub> species is one of the important reasons for greater adsorption at lower weak acid pH. Iida et al. [4] have reported that activated alumina surface is positively charged in the range from pH value of 3 to 6 and, consequently, anionic MO ions can be adsorbed on acidic sites of alumina with positive charge. In this regard, MO molecules can be adsorbed on the ZnO nanoflakes together with Al<sub>2</sub>O<sub>3</sub> particles at weak acid pH.

As can be clearly seen in Fig. 6, there was a significant reduction when pH further decreased to 2.6. This significant reduction below the pH value of 3 can be related to dissolution of ZnO–Al<sub>2</sub>O<sub>3</sub> particles in strong acidic media, which is in agreement with other studies [4,14,20]. In our study, it was concluded that the weak acid pH is the ideal pH for MO adsorption on ZnO–Al<sub>2</sub>O<sub>3</sub> nanocomposite adsorbent. Moreover, the pH value of 4.5 was achieved as the optimum pH for the present work, which is far enough from the region of strong acidic pH.

### 3.5. Adsorption kinetics

Kinetic modeling is widely applied to estimate the adsorption rate and to investigate the controlling mechanisms of adsorption reaction such as mass transfer, diffusion control, and chemical reaction, which are important in designing an adsorption treatment plant [17]. In this regard, three most widely used kinetic models including Lagergren-first-order equation [3], pseudo-second-order equation [17], and intra-particle diffusion model [21] were used to test the experimental data and recognize the characteristics of

adsorption mechanism of MO dye on ZnO–Al<sub>2</sub>O<sub>3</sub> nanocomposite particles from aqueous solution.

The Lagergren-first-order model is based on the assumption that the rate of change of solute uptake over time is directly proportional to the difference in saturation concentration and the amount of solid uptake over time [3]. Hence, the Lagergren-first-order kinetic model is expressed by the following equation:

$$\frac{dq_t}{dt} = K_1(q_e - q_t) \quad (3)$$

By integrating Eq. (3) and noting the boundary condition  $q_t=0$  at  $t=0$ , the linear form of Lagergren-first-order model is expressed as:

$$\log(q_e - q_t) = \log q_e - \frac{K_1}{2.303}t \quad (4)$$

where  $q_e$  and  $q_t$  are the amounts of MO adsorbed on per unit mass of adsorbent at equilibrium and time  $t$  (in mg/g), respectively.  $K_1$  is the Lagergren-first-order rate constant (in 1/min).

The pseudo-second-order kinetic model is based on the assumption that the dye molecules get adsorbed onto two surface sites of adsorbent [22]. Accordingly, the pseudo-second-order kinetic model is represented as:

$$\frac{dq_t}{dt} = K_2(q_e - q_t)^2 \quad (5)$$

Integrating Eq. (5) at boundary condition  $q_t=0$  at  $t=0$ , gives the following linear form:

$$\frac{t}{q_t} = \frac{1}{K_2q_e^2} + \frac{1}{q_e}t \quad (6)$$

where  $q_e$  and  $q_t$  are the amounts of MO adsorbed on per unit mass of adsorbent at equilibrium and time  $t$  (in mg/g), respectively.  $K_2$  is the pseudo-second-order rate constant (in g/[mg min]). The initial adsorption rate  $h_0$  (in mg/[g min]) at  $t \rightarrow 0$  is defined as:

$$h = K_2q_e^2 \quad (7)$$

In order to fit the kinetic models at optimum conditions obtained from the previous batch adsorption experiments, the kinetic studies in terms of time, percentage removal, and adsorption capacity (not shown here, like previous batch adsorption experiments) were carried out at optimum pH value of 4.5 for different dye concentrations ranging from 100 to 200 ppm and fixed adsorbent concentration of 500 ppm. The rate constants ( $K_1$  and  $K_2$ ) and other kinetic parameters were determined from the slope and intercept of the linear plot of  $\log(q_e - q_t)$  vs.  $t$  for Lagergren-first-order model and the linear plot of  $t/q_t$  vs.  $t$  for pseudo-second-order model (see Fig. 7). The rate constant of adsorption and other calculated kinetic parameters for both models along with the corresponding linear regression correlation coefficient  $R^2$  and related experimental data are given in Table 1. The fitting between experimental data and kinetic

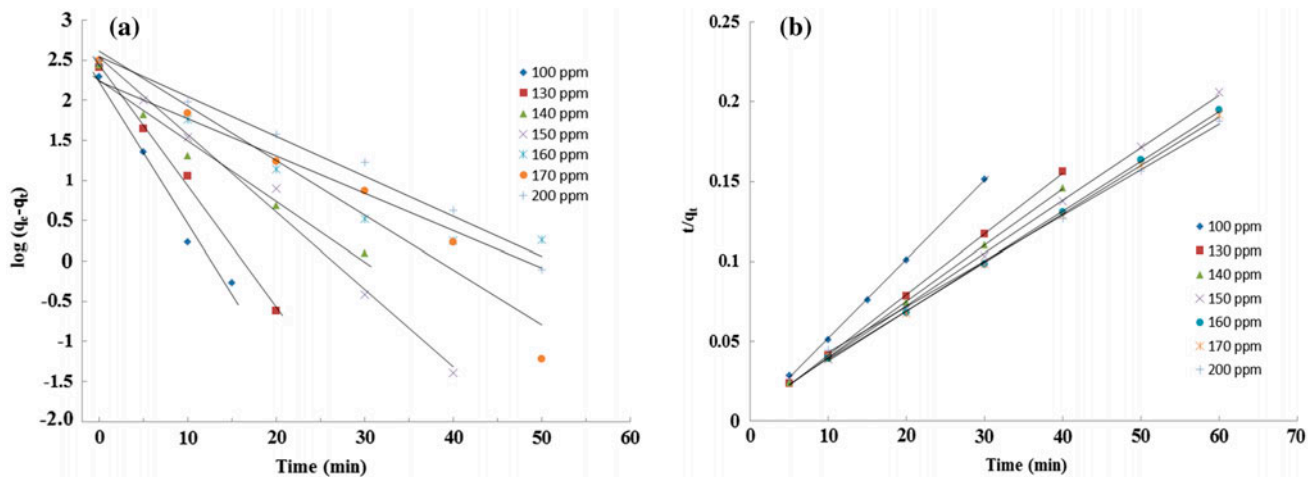


Fig. 7. Lagergren-first-order kinetic model (a) and pseudo-second-order kinetic model (b) for the adsorption of MO on ZnO–Al<sub>2</sub>O<sub>3</sub> nanocomposite adsorbent (initial MO concentration of 100–200 ppm, adsorbent concentration of 500 ppm, pH value of 4.5).

Table 1

Kinetic parameters calculated from Lagergren-first-order model and pseudo-second-order model and experimental data for MO adsorption

$C_0$ (mg/L)	$\eta$ (%)	$q_{e,exp}$ (mg/g)	Lagergren-first-order kinetic model			Pseudo-second-order kinetic model				
			$q_{e1,cal}$ (mg/g)	$K_1$ (1/min)	$R^2$	$q_{e2,cal}$ (mg/g)	$K_2$ (g/[mg min])	$h_0$ (mg/[g min])	$R^2$	
100	99	197.38	168.31	0.4058	0.9799	204.08	0.0092	384.615	0.9996	
130	98	255.20	272.65	0.3461	0.9961	263.16	0.0041	285.714	0.9997	
140	98	272.70	176.77	0.1734	0.9730	285.71	0.0023	192.308	0.9996	
150	97	290.94	339.70	0.2215	0.9907	303.03	0.0016	151.515	0.9991	
160	95	306.28	171.71	0.1071	0.9198	322.58	0.0015	151.515	0.9994	
170	92	312.76	406.63	0.1566	0.9515	333.33	0.0011	117.647	0.9992	
200	80	318.76	354.73	0.1149	0.9837	344.83	0.0059	69.930	0.9992	

model was examined by correlation coefficient value of  $R^2$  and the comparison of experimental and calculated value of  $q_e$ .

As can be seen in Table 1, the correlation coefficient  $R^2$  for pseudo-second-order kinetic model is higher than that of the Lagergren-first-order kinetic model for different initial dye concentrations. Also, the calculated  $q_{e2,cal}$  values obtained from the pseudo-second-order model are in better agreement with the experimental  $q_{e,exp}$  values for all initial dye concentrations. Therefore, these results confirm that the pseudo-second-order kinetic model have described more appropriately the kinetic of MO adsorption on ZnO–Al<sub>2</sub>O<sub>3</sub> nanocomposite particles. As a result, it is suggested that the present adsorption mechanism be more controlled by rate-limiting step of the chemisorption compared to mass transfer in the solution [14,17]. According to Table 1, it was found that the initial adsorption rate decreases by enhancing the initial MO concentration. Indeed, this phenomenon can be related to the involvement of mass transfer in solution due to the presence of more MO molecules in solution at higher concentrations, which lengthens the equilibrium time. However, this result stands against the rate-limiting step of the chemisorption predicted by pseudo-second-order model. Hence, it may be concluded that there is a serious competition between the chemisorption and mass transfer in solution for controlling the rate-limiting step of adsorption process. It should be mentioned that the same results related to real complexities and problems in estimating the kinetic parameters by linearization technique of pseudo-second-order model were reported by Vasanth Kumar [22].

In general, the following four steps are considered to be involved in the adsorption process of a dye on the surface of an adsorbent [19]:

- (1) The dye molecules mass transfer from bulk solution to the surface of adsorbent (bulk diffusion mass transfer).
- (2) Diffusion of dye molecules through boundary layer to the surface of adsorbent (film diffusion mass transfer or boundary layer).
- (3) Diffusion of dye molecules from the surface of adsorbent to the interior pores of particle (intraparticle diffusion mass transfer).
- (4) Chemical or physical adsorption of dye molecules on active sites of the adsorbent surface (adsorption reaction).

Generally, at liquid–solid systems for dye adsorption process, the mass transfer in bulk solution is quit rapid and hence it cannot be the rate-determining step. Also, the chemisorption step is not a suitable rate-limiting step for MO adsorption process on present ZnO–Al<sub>2</sub>O<sub>3</sub> nanocomposite adsorbent due to its great affinity and superior activity for adsorption of MO molecules which have been previously confirmed [13,20]. Therefore, dye adsorption is more governed by mass transfer (whether film diffusion or intraparticle diffusion), which is relatively in agreement with the results obtained from pseudo-second-order kinetic model (referring to the presence of competing mass transfer) and other studies by other researchers [14,17,20]. In order to achieve more accurate interpretation of the adsorption mechanisms affecting the adsorption kinetic, the intraparticle diffusion model proposed by Weber and Morris was applied [23]:

$$q_t = k_i t^{0.5} + C_2 \quad (8)$$

where  $q_t$  is the amount of MO adsorbed on per unit mass of adsorbent at equilibrium time  $t$  (in mg/g).  $k_i$  is the intraparticle diffusion rate constant

[in  $\text{mg}/[\text{g min}^{0.5}]$ ].  $C$  is the adsorption constant that represents the thickness of boundary layer. The plot of  $q_t$  vs.  $t^{0.5}$  should theoretically give a straight line in which  $k_i$  is the slope and  $C_2$  is the intercept. If the plot was found to be linear, it could imply that the intraparticle diffusion is the rate-controlling step, and if it passed from the origin, it can be indicated that the intraparticle diffusion is the only rate-controlling step. In addition, the greater intercept means that greater contribution of boundary layer effect is involved in the rate-controlling step. The experimental data together with intraparticle diffusion model in terms of  $q_t$  vs.  $t^{0.5}$  are shown in Fig. 8. It is obvious that the plot is not linear over the whole time range for all initial concentrations. Besides, a more careful observation shows that the plot can be divided into two portions, indicating that multiple mechanisms are involved in the adsorption process. The first portion seems to be a curve to pass through the origin. The curved portion implied the boundary layer effect in the rate-controlling step, which continued until  $\sim 13$  min ( $t^{0.5} = 3.6$ ). Furthermore, the very high and positive value of slope of the dashed line indicated that a rapid adsorption occurs within a short period of time. The second portion represented a linear portion, which was suitably fitted to intraparticle diffusion model. It should be noted that this linear portion does not pass through the origin, indicating that the intraparticle diffusion is not the only rate-controlling step. The linear portion starts from the time of  $\sim 13$  min and then gets a longer time period of the adsorption process. Also, compared to the first portion of the plot, the second portion has a lower slope, indicating that the second portion controlled by intraparticle diffusion is much slower than the film diffusion and hence, its rate is not quite rapid.

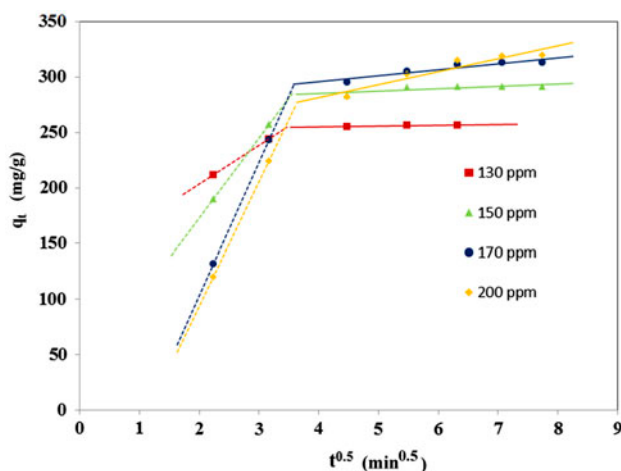


Fig. 8. Intraparticle diffusion model for MO adsorption on  $\text{ZnO-Al}_2\text{O}_3$  nanocomposite adsorbent.

Table 2

The parameters evaluated from intraparticle diffusion model for MO adsorption

$C_0$ (mg/L)	$k_{i,2}$ ( $\text{mg}/[\text{g min}^{0.5}]$ )	$C_2$ (mg/g)
130	0.6553	252.45
150	2.1461	276.34
170	5.3500	274.24
200	11.6100	235.37

Concerning that neither portions of the plot passed through the origin, it can be concluded that both film diffusion and intraparticle diffusion are simultaneously occurring during the adsorption process [23]. These results are in agreement with other studies [3,17,24]. The values of  $C$  and the rate constant  $k_i$  were evaluated from the intercept and the slope of the linear portion (obtained from intraparticle diffusion model), and are given in Table 2. As listed, by increasing the initial MO concentration, the diffusion rate constant  $k_i$  increases, which would be expected due to the enhancement of the concentration gradient of MO (driving force) at a higher concentration. Moreover, by increasing the initial MO concentration, the value of  $C$  (boundary layer or film diffusion effect) first shows a little enhancement and then is followed by an intense reduction. This phenomenon means that the structure of  $\text{ZnO-Al}_2\text{O}_3$  nanocomposite adsorbent is stable against the boundary layer effect and hence keeps an appropriate diffusion rate of MO in the boundary layer, while in some studies [3,14,17], the value of  $C$  sharply increases by increasing the initial dye concentration. Here, lack of a sharp increase in the value of  $C$  by increasing the initial MO concentration can be attributed to the high surface area of the adsorbent and the activated surface charge of  $\text{ZnO}$  nanosized active sites (Fig. 2), which both generate a high affinity of surface sites for the attraction of MO ions [13].

### 3.6. Adsorption isotherms

In order to describe the behavior and performance of the adsorption process, two well-known adsorption isotherm models of Langmuir and Freundlich were used [15,17]. The Langmuir isotherm model is based on a saturated monolayer of solute molecules on the active sites of the adsorbent surface. The Freundlich isotherm model is based on the assumption that the adsorption surface becomes heterogeneous during the course of the adsorption process. The linear forms of both models and their related correlation coefficients were applied to determine the best-fitting isotherm and to establish the adsorption isotherm constants.

The Freundlich isotherm is represented by the following empirical equation:

$$q_e = K_F C_e^{1/n} \quad (9)$$

By taking a logarithm, the linearized form of Eq. (9) can be described as follows:

$$\log q_e = \log K_F + \frac{1}{n} \log C_e \quad (10)$$

where  $q_e$  is the amount of dye adsorbed on per unit mass of adsorbent at equilibrium (in mg/g),  $K_F$  constant is the adsorption coefficient and is related to adsorption capacity of MO dye on adsorbent at equilibrium concentration,  $C_e$  is the MO concentration in solution at equilibrium (in mg/L), and  $n$  is another adsorption constant and is related to adsorption intensity of MO molecules on adsorbent surface.  $1/n$  gives an indication of how favorable the adsorption process is. Values of  $n > 1$  represent favorable adsorption conditions indicating a normal Langmuir isotherm [24].

The Langmuir isotherm model is given by the following equation:

$$q_e = \frac{q_m K_L C_e}{1 + K_L C_e} \quad (11)$$

The linear form of Eq. (11) can be represented as:

$$\frac{1}{q_e} = \frac{1}{q_m} + \frac{1}{K_L q_m} \frac{1}{C_e} \quad (12)$$

where  $q_e$  is the amount of dye adsorbed on per unit mass of adsorbent at equilibrium (in mg/g),  $q_m$  is the theoretical amount of maximum adsorption with complete monolayer coverage on the adsorbent surface (in mg/g),  $C_e$  is the concentration of dye solution at equilibrium (in mg/L), and  $K_L$  is the Langmuir isotherm constant (in L/mg). The  $K_L$  constant is related to the energy of adsorption sites.

Also the essential characteristics of the Langmuir isotherm can be described in terms of a dimensionless constant separation factor  $R_L$  that is given by the following equation [25].

$$R_L = \frac{1}{1 + K_L C_0} \quad (13)$$

where  $C_0$  is the highest initial concentration of dye (in mg/L) and  $K_L$  is the Langmuir isotherm constant (in L/mg). The value of  $R_L$  indicates the shape of the isotherm to be either unfavorable ( $R_L > 1$ ), linear ( $R_L = 1$ ), favorable ( $0 < R_L < 1$ ), or irreversible ( $R_L = 0$ ).

According to linear forms of Langmuir and Freundlich isotherms, the plot of  $\log(q_e)$  vs.  $\log(C_e)$  and the plot of  $1/q_e$  vs.  $1/C_e$  were considered to determine isotherm constants and other corresponding parameters. The linear and nonlinear plots of both models were separately depicted in Fig. 9, and related constants and parameters are given in Table 3.

According to Fig. 9(a) and (b) and Table 3, the correlation coefficient  $R^2$  is high for Langmuir isotherm model ( $R^2 = 0.9784$ ) compared to Freundlich isotherm model ( $R^2 = 0.7068$ ). Thus, the adsorption behavior of MO on ZnO–Al<sub>2</sub>O<sub>3</sub> nanocomposite is best fitted to Langmuir isotherm model. This fitting can be clearly seen from nonlinear plots depicted in Fig. 9(c),

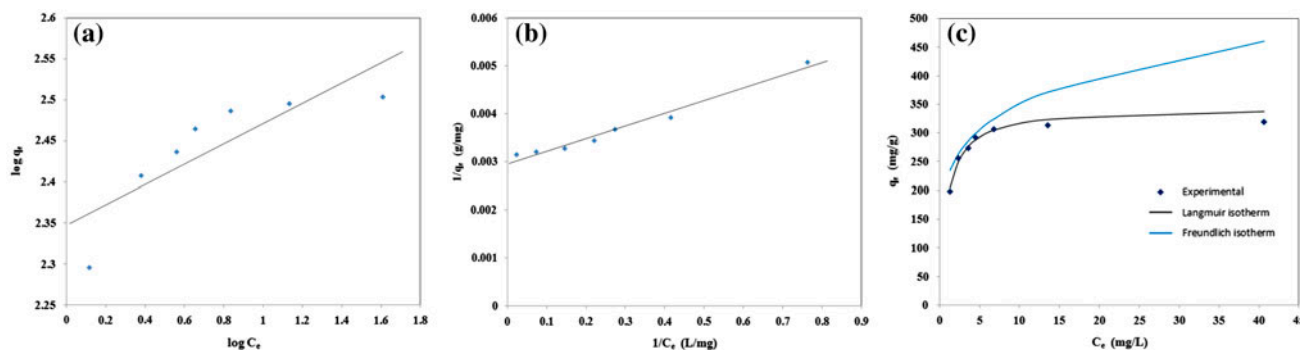


Fig. 9. Linear Freundlich and Langmuir adsorption isotherm (a and b, respectively) and nonlinear plots of both models (c) for the adsorption of MO on ZnO–Al<sub>2</sub>O<sub>3</sub> nanocomposite adsorbent (initial MO concentration of 100–200 ppm, adsorbent concentration of 500 ppm, pH value of 4.5).

Table 3  
Freundlich and Langmuir isotherm constants and correlation coefficients for the adsorption of MO on ZnO–Al<sub>2</sub>O<sub>3</sub> nanocomposite adsorbent

Isotherm	Parameters
<i>Langmuir model</i>	
$q_m$ (mg/g)	344.83
$K_L$ (L/mg)	1.1154
$R^2$	0.9784
$R_L$	0.0045
<i>Freundlich model</i>	
$K_F$ (mg/g [L/g] <sup>1/n</sup> )	222.5871
$n$	5.0972
$R^2$	0.7068

indicating a high affinity of ZnO–Al<sub>2</sub>O<sub>3</sub> nanocomposite particle surfaces for adsorption of MO dye, especially at low MO concentrations. Also, the fitted Langmuir isotherm can refer to homogeneity of ZnO–Al<sub>2</sub>O<sub>3</sub> nanocomposite surfaces in terms of distribution of active sites for the adsorption of a monolayer of MO molecules on the adsorbent surface. This result has also been reported by other researchers for MO adsorption on different adsorbents [3,17,24]. According to Langmuir isotherm model, the theoretical amount of maximum monolayer adsorption capacity ( $q_m$ ) was calculated as 344.83 mg/g. As can be seen in Table 3, the value of  $R_L$  was found to be 0.0045. The obtained value of  $R_L$  indicated that the MO monolayer adsorption on the adsorbent surface was a favorable adsorption. However, the very near zero value of  $R_L$  may imply an irreversible adsorption process of MO molecules on active sites.

Table 4  
Comparison of MO adsorption using present ZnO–Al<sub>2</sub>O<sub>3</sub> nanocomposite adsorbent with other adsorbents at room temperature

Adsorbent	Theoretical $q_{m,theo}$	Experimental $q_{m,exp}$ (at $\eta > 90\%$ )	Ref.
ZnO–Al <sub>2</sub> O <sub>3</sub> nanocomposite	344.83	291 ( $\eta = 97\%$ )	This study
ZnO–Al <sub>2</sub> O <sub>3</sub> nanocomposite	344.83	312.76 ( $\eta = 92\%$ )	This study
Lapindo volcanic mud	333.33	110.26	[3]
$\gamma$ -Fe <sub>2</sub> O <sub>3</sub> /SiO <sub>2</sub> /CS composite	34.29	–	[14]
Activated alumina	–	9.8	[4]
Calcined MgNiAl	375.4	47.7	[17]
De-oiled soya	13.46	–	[19]
Bottom ash	3.62	–	[19]
Zn/Al layered	200	181.9	[20]
Multiwalled carbon nanotubes	51.74	–	[26]
Modified nanosize SiO <sub>2</sub> –Al <sub>2</sub> O <sub>3</sub>	381.0	~19	[27]

The most common parameter to compare the dye adsorption capacity is the Langmuir theoretical maximum adsorption capacity ( $q_m$ ), of course, regardless of the percentage removal of dye at maximum adsorption. In this regard, in order to compare the adsorption capacity of MO on ZnO–Al<sub>2</sub>O<sub>3</sub> nanocomposite with other low-cost adsorbents reported by other researchers, the experimental amount of maximum adsorption capacity at percentage removal of MO dye above 90% ( $q_{m,exp}$ ) together with the theoretical amount of Langmuir maximum adsorption capacity ( $q_{m,theo}$ ) are listed in Table 4. However, it should be noted that the  $q_{m,exp}$  is more realistic than  $q_{m,theo}$ . As can be seen, regarding both reported  $q_{m,exp}$  and  $q_{m,theo}$  values, the ZnO–Al<sub>2</sub>O<sub>3</sub> nanocomposite adsorbent has a relatively superior adsorption capacity than other adsorbents. Therefore, it can be concluded that the low-cost ZnO–Al<sub>2</sub>O<sub>3</sub> nanocomposite is a suitable and promising adsorbent for the removal of the azo dyes in industrial wastewater treatment.

#### 4. Conclusion

ZnO–Al<sub>2</sub>O<sub>3</sub> nanocomposite particles were utilized as adsorbent for MO dye removal from an aqueous solution. Batch adsorption experiments confirmed that MO adsorption on nanocomposite particles highly depended on the dye concentration, adsorbent concentration, and solution pH. The best result was obtained at the dye concentration of 150 ppm, adsorbent concentration of 500 ppm, and the pH value of 4.5 with 97% dye removal and adsorption capacity of 291 mg/g in a low equilibrium time of 30 min. The pseudo-second-order and intraparticle diffusion kinetic models described the adsorption kinetics of MO on the present adsorbent. According to kinetic

evaluations, it was found that the MO adsorption process is mainly controlled by the intraparticle diffusion and film diffusion mechanism and both parameters occurred simultaneously. The adsorption isotherm was well represented by Langmuir isotherm model, indicating a high affinity of ZnO–Al<sub>2</sub>O<sub>3</sub> nanocomposite particles surfaces for adsorption of MO dye. Finally, according to the mentioned results, ZnO–Al<sub>2</sub>O<sub>3</sub> nanocomposite particles can be used as an inexpensive alternative adsorbent for the removal of azo dyes in industrial wastewater treatment.

## References

- [1] K.Y. Foo, B.H. Hameed, An overview of dye removal via activated carbon adsorption process, *Desalin. Water Treat.* 19 (2010) 255–274.
- [2] W.S. Wan Ngaha, L.C. Teonga, M.A.K.M. Hanafiah, Adsorption of dyes and heavy metal ions by chitosan composites: A review, *Carbohydr. Polym.* 83 (2011) 1446–1456.
- [3] A.A. Jalil, S. Triwahyono, S. Adam, N. Rahim, M.A.A. Aziz, N.H. Hairom, N.A.M. Razali, M.A.Z. Abidin, M.K.A. Mohamadiah, Adsorption of methyl orange from aqueous solution onto calcined Lapindo volcanic mud, *J. Hazard. Mater.* 181 (2010) 755–762.
- [4] Y. Iida, T. Kozuka, T. Tuziuti, K. Yasui, Sonochemically enhanced adsorption and degradation of methyl orange with activated aluminas, *Ultrasonics* 42 (2004) 635–639.
- [5] T. Zhang, Q. Li, Z. Mei, H. Xiao, H. Lu, Y. Zhou, Adsorption of fluoride ions onto non-thermal plasma-modified CeO<sub>2</sub>/Al<sub>2</sub>O<sub>3</sub> composites, *Desalin. Water Treat.* 52 (2014) 3367–3376.
- [6] H.Y. Zhang, G. Shan, H.Z. Liu, J.M. Xing, Preparation of (Ni/W)- $\gamma$ -Al<sub>2</sub>O<sub>3</sub> microspheres and their application in adsorption desulfurization for model gasoline, *Chem. Eng. Commun.* 194 (2007) 938–945.
- [7] G. McKay, M. Hadi, M.T. Samadi, A.R. Rahmani, M. Aminabad, F. Nazemi, Adsorption of reactive dye from aqueous solutions by compost, *Desalin. Water Treat.* 28 (2011) 164–173.
- [8] J.X. Lin, L. Wang, Adsorption of dyes using magnesium hydroxide-modified diatomite, *Desalin. Water Treat.* 8 (2009) 263–271.
- [9] P. Bansal, N. Bhullar, D. Sud, Studies on photodegradation of malachite green using TiO<sub>2</sub>/ZnO photocatalyst, *Desalin. Water Treat.* 12 (2009) 108–113.
- [10] Z.L. Wang, Zinc oxide nanostructures: Growth, properties and applications, *J. Phys.: Condens. Matter* 16 (2004) 829–858.
- [11] X. Qu, D. Jia, Controlled growth and optical properties of Al<sup>3+</sup> doped ZnO nanodisks and nanorod clusters, *Mater. Lett.* 63 (2009) 412–414.
- [12] J.C. Chen, C.T. Tang, Preparation and application of granular ZnO/Al<sub>2</sub>O<sub>3</sub> catalyst for the removal of hazardous trichloroethylene, *J. Hazard. Mater.* 142 (2007) 88–96.
- [13] H. Tajizadegan, M. Jafari, M. Rashidzadeh, A. Saffar-Teluri, A high activity adsorbent of ZnO–Al<sub>2</sub>O<sub>3</sub> nanocomposite particles: Synthesis, characterization and dye removal efficiency, *Appl. Surf. Sci.* 276 (2013) 317–322.
- [14] H.Y. Zhu, R. Jiang, Y.Q. Fu, J.H. Jiang, L. Xiao, G.M. Zeng, Preparation, characterization and dye adsorption properties of  $\gamma$ -Fe<sub>2</sub>O<sub>3</sub>/SiO<sub>2</sub>/chitosan composite, *Appl. Surf. Sci.* 258 (2011) 1337–1344.
- [15] N. Barka, S. Qourzal, A. Assabbane, A. Nounah, Y. Ait-Ichou, Removal of Reactive Yellow 84 from aqueous solutions by adsorption onto hydroxyapatite, *J. Saudi. Chem. Soc.* 15 (2011) 263–267.
- [16] N. Yousefi, A. Fatehizadeh, E. Azizi, M. Ahmadian, A. Ahmadi, A. Rajabizadeh, A. Toolabi, Adsorption of reactive black 5 dye onto modified wheat straw: Isotherm and kinetics study, *Sacha. J. Environ. Stud.* 1 (2011) 81–89.
- [17] H. Zaghouane-Boudiaf, M. Boutahala, L. Arab, Removal of methyl orange from aqueous solution by uncalcined and calcined MgNiAl layered double hydroxides (LDHs), *Chem. Eng. J.* 187 (2012) 142–149.
- [18] M.S. Mashkour, A.F. Al-Kaim, L. Ahmed, F.H. Hussein, Zinc oxide assisted photocatalytic decolorization of reactive red 2 dye, *Int. J. Chem. Sci.* 9 (2011) 969–979.
- [19] A. Mittal, A. Malviya, D. Kaur, J. Mittal, L. Kurup, Studies on the adsorption kinetics and isotherms for the removal and recovery of Methyl Orange from wastewaters using waste materials, *J. Hazard. Mater.* 148 (2007) 229–240.
- [20] Z.M. Ni, S.J. Xia, L.G. Wang, F.F. Xing, G.X. Pan, Treatment of methyl orange by calcined layered double hydroxides in aqueous solution: Adsorption property and kinetic studies, *J. Colloid. Interface Sci.* 316 (2007) 284–291.
- [21] F.C. Wu, R.L. Tseng, R.S. Juang, Initial behavior of intraparticle diffusion model used in the description of adsorption kinetics, *Chem. Eng. J.* 153 (2009) 1–8.
- [22] K. Vasanth Kumar, Linear and non-linear regression analysis for the sorption kinetics of methylene blue onto activated carbon, *J. Hazard. Mater.* 137 (2006) 1538–1544.
- [23] B.K. Nandi, A. Goswami, M.K. Purkait, Adsorption characteristics of brilliant green dye on kaolin, *J. Hazard. Mater.* 161 (2009) 387–395.
- [24] W.J. Weber Jr., J.C. Morris, Kinetics of adsorption on carbon from solution, *J. Sanit. Eng. Div.* 89 (1963) 3–60.
- [25] B.H. Hameed, D.K. Mahmoud, A.L. Ahmad, Equilibrium modeling and kinetic studies on the adsorption of basic dye by a low-cost adsorbent: Coconut (*Cocos nucifera*) bunch waste, *J. Hazard. Mater.* 158 (2008) 65–72.
- [26] Y. Yao, H. Bing, X. Feifei, C. Xiaofeng, Equilibrium and kinetic studies of methyl orange adsorption on multiwalled carbon nanotubes, *Chem. Eng. J.* 170 (2011) 82–89.
- [27] M. Arshadi, F. Salimi Vahid, J.W.L. Salvacion, M. Soleymanzadeh, A practical organometallic decorated nano-size SiO<sub>2</sub>–Al<sub>2</sub>O<sub>3</sub> mixed-oxides for methyl orange removal from aqueous solution, *Appl. Surf. Sci.* 280 (2013) 726–736.